ACSNANO
www.acsnano.org
ARTICLE

Tuning the Selectivity of Dendron Micelles Through Variations of the Poly(ethylene glycol) Corona

Ryan M. Pearson,[†] Soumyo Sen,[§] Hao-jui Hsu,[†] Matt Pasko,[†] Marilyn Gaske,[†,§] Petr Král,[§,∥] and Seungpyo Hong*[,†,‡,⊥,#]

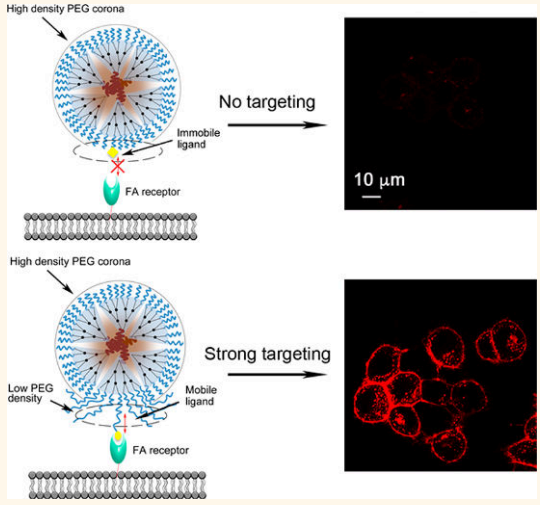
[†]Department of Biopharmaceutical Sciences, College of Pharmacy, University of Illinois at Chicago, Chicago, Illinois 60612, United States

Departments of [‡]Bioengineering, [§]Chemistry, and [∥]Physics, University of Illinois at Chicago, Chicago, Illinois 60607, United States

[⊥]Department of Integrated OMICs for Biomedical Science and [#]Underwood International College, Yonsei University, Seoul, 03706, Republic of Korea

Supporting Information

ABSTRACT: **Engineering controllable cellular interactions into nanoscale drug delivery systems is key to enable their full potential. Here, using folic acid (FA) as a model targeting ligand and dendron micelles (DM) as a nanoparticle (NP) platform, we present a comprehensive experimental and modeling investigation of the structural properties of DMs that govern the formation of controllable, FA-mediated cellular interactions. Our experimental results demonstrate that a high level of control over the specific cell interactions of FA-targeted DMs can be achieved through modulation of the PEG corona length and the FA content. Using various molecular weight PEGs (0.6K, 1K, and 2K g/mol) and contents of dendron-FA conjugate incorporated into DMs (0, 5, 10, 25 wt %), the cell interactions of the targeted DMs could be controlled to exhibit minimal to >25-fold enhancement over nontargeted DMs. Molecular dynamics simulations indicated that structural characteristics, such as solvent accessible surface area of FA, local PEG density near FA, and FA mobility, account in part for the experimental differences in cellular interactions. The molecular structure that allows FA to depart from the surface of DMs to facilitate the initial cell surface binding was revealed to be the most important contributor for determining FA-mediated cellular interactions of DMs. The modular properties of DMs in controlling their specific cell interactions support the potential of DMs as a delivery platform and offer design cues for future development of targeted NPs.**



KEYWORDS: *dendron micelle, targeted drug delivery, PEG corona, self-assembly*

Establishing methods to achieve precise control over cellular interactions of nanoparticles (NP) is important to enhance their therapeutic efficacy and will ultimately impact their successful clinical translation, particularly in personalized medicine.[1−3] PEGylation, or surface grafting of poly(ethylene glycol) (PEG) to NPs, has been widely employed to reduce the formation of nonspecific cellular interactions and minimize serum protein binding in a density-dependent manner.[4−7] On the other hand, the attachment of targeting ligands, such as antibodies, aptamers, peptides, sugars, and small molecules, to the distal ends of PEG chains can impart cell-specific binding properties to NPs and promote targeted drug delivery.[8,9] However, evidence has accumulated suggesting that, although useful for minimizing nonspecific interactions, the use of high density PEG (brush-like conformation in particular) can hinder the formation of targeted cellular interactions as it restricts the surface accessibility and availability of the targeting ligand.[4,10,11] Approaches to overcoming those adverse effects of PEG or the so-called "PEG dilemma" include conjugation of targeting ligands to PEG tethers in order to allow for an unhindered

Received: April 22, 2016
Accepted: June 6, 2016
Published: June 6, 2016

© 2016 American Chemical Society

DOI: 10.1021/acsnano.6b02708
ACS Nano 2016, 10, 6905−6914

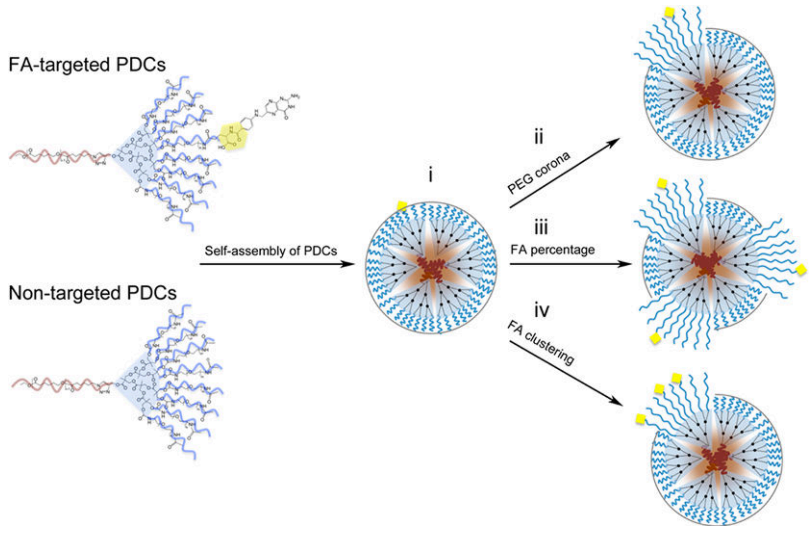


Figure 1. Systematic evaluation of the FA-targeted cellular interactions of DMs. FA-targeted PDCs were mixed with nontargeted PDCs at various ratios to evaluate the effect of the PEG corona length, FA percentage, and FA clustering on the formation of targeted cellular interactions.

interaction between surface-bound targeting ligands and their binding counterparts on the cell membrane.[7,10,12−17] However, the relationship between physicochemical parameters of PEGylated, targeted NPs and their cellular interactions remains largely unexplored, hindering the design of an effective NP system that possesses controllable and consistent cellular interactions.

Recognizing the need for NPs to maintain high density PEG layers to promote the "stealth" effect, and yet realize high affinity and modular cellular interactions, we have recently developed dendron micelles (DM).[18−20] DMs are self-assembled nanostructures prepared from PEGylated dendron-based copolymers (PDC) that are amphiphilic triblock copolymers comprised of linear and dendritic polymer components (Figure 1). The dendritic component (generation 3 polyester dendron) of PDCs enables multiple PEG chains to be conjugated to a single copolymer, resulting in DMs with strongly pronounced, high-density surface presentation of PEG layers. We previously reported that changes in the PEG corona lengths of DMs affected their nonspecific, charge-dependent cellular interactions in a controllable manner. For example, amine-terminated, positively charged DMs with PEG with molecular weight of 2000 g/mol (PEG2K) chains displayed negligible cellular interactions,[19] whereas similar DMs with shorter PEG0.6K formed strong nonspecific cellular interactions,[20] which was in agreement with a recent study using PEGylated Au NPs.[21] These findings support that DMs are an ideal platform to study the role of surface-bound molecules and PEG chains on the formation of controllable and targeted cellular interactions of NPs.

In this paper, we systematically evaluate the roles played by nanoscale structural features, including PEG corona length and targeting ligand density and clustering, on cellular interactions of DMs. Based on our previous results and literature, this study proceeds by testing three hypotheses: (1) shortening of the PEG corona length conjugated with a targeting ligand can amplify the targeting of DMs by intensifying the end-group effect; (2) increasing the number of targeting ligands incorporated into DMs would enhance the targeting ability of DMs; and (3) clustering of targeting ligands on the surface of DMs in a similar manner to dendrimers[22,23] and linear-dendritic block copolymer (LDBC) micelles[24] would facilitate the formation of localized multivalent interactions and enhance the cellular interactions of DMs. Surprisingly, each of these hypotheses was independently disproven; however, methods to modulate the level of targeted cellular interactions achieved by DMs were uncovered. Our experimental findings were further explained using atomistic molecular dynamics (MD) simulations that provided quantitative understanding of the cell interactions of the targeted DMs. It is expected that the findings presented herein will be useful for the development of the next generation of targeted NPs by providing methods to modulate NP-mediated specific cellular interactions.

RESULTS AND DISCUSSION

Given that folate receptors (FR) are overexpressed by a variety of cancer cells and that folic acid (FA) has been widely investigated to improve targeting of NPs,[25−27] FA was employed as the model targeting ligand in this study to interrogate the targeted cellular interactions of DMs. FA-targeted PDCs with different PEG chain lengths (0.6K and 2K g/mol) were synthesized by coupling *N*-hydroxysuccinimide activated FA to amine-terminated PDCs.[28] After FA conjugation, the remaining primary amine groups on PDCs were acetylated to block the formation of nonspecific interactions with cell membranes (Figure S1 of the Supporting Information).[20] ^{1}H NMR and UV−vis data revealed that 1, 2, or 3 FA molecules were conjugated to individual PDCs denoted as PDC-FA_1, PDC-FA_2, and PDC-FA_3, respectively. Nontargeted PDCs without FA were also synthesized using our previously reported protocols,[18−20] where PDCs were prepared with PEG chains of 0.6K, 1K, and 2K g/mol. Details of the PDCs synthesized for this study including synthetic methods and characterization data obtained using ^{1}H NMR and GPC can be found in the Supporting Information (Figures S2−3 and Table S1).

FA-targeted DMs were prepared by self-assembly from mixtures of targeted PDCs (PDC0.6K-FA_1, PDC0.6K-FA_2, PDC2K-FA_1, or PDC2K-FA_3) and nontargeted PDCs (PDC0.6K, PDC1K, or PDC2K) at various ratios to evaluate

DOI: 10.1021/acsnano.6b02708
ACS Nano 2016, 10, 6905−6914

the effect of the PEG corona length, percentage of PDC-FA incorporation, and FA clustering on the formation of targeted cellular interactions (Figure 1 and Table 1). For detection of cellular interactions of DMs by fluorescence-based techniques, each formulation contained 10 wt % of Rho-labeled PDC0.6K.[20] All DMs were found to have similar sizes (~20 nm in hydrodynamic diameter) as measured using dynamic light scattering (DLS) and ζ potentials varying from −8.2 to 0.2 mV (Table 1 and Figure S4 of the Supporting Information).

Table 1. Size and ζ Potential Measurements of Dendron Micelle Formulations

micelles	PEG corona	PEG-FA	PDC-FA (wt %)	size ± SD (nm)	ZP ± SD (mV)
DM1	0.6K	0.6K	0	17.3 ± 3.7	−5.7 ± 0.3
DM2	0.6K	0.6K	5	23.8 ± 5.1	−7.5 ± 2.2
DM3	0.6K	2K	5	22.2 ± 4.4	0.2 ± 0.7
DM4	0.6K	2K	10	22.7 ± 4.0	−8.2 ± 0.8
DM5	0.6K	2K	25	23.9 ± 5.0	−4.2 ± 4.7
DM6	1K	2K	0	23.8 ± 5.3	−3.0 ± 4.3
DM7	1K	2K	5	20.7 ± 4.1	−0.6 ± 0.5
DM8	1K	2K	10	17.2 ± 3.6	−4.5 ± 2.8
DM9	1K	2K	25	15.4 ± 2.9	−6.0 ± 0.8
DM10	2K	2K	5	23.1 ± 4.0	−3.6 ± 2.4

The first hypothesis was set up based on our previous finding where DMs with PEG0.6K chains (DM0.6K) exhibited a pronounced end-group effect on their cellular interactions.[20] To assess hypothesis 1 (Figure 1i) that shortening the PEG corona length would facilitate the formation of strong, targeted cellular interactions of DMs, we monitored cell interactions of FA-targeted DM0.6K with FR-overexpressing KB cells (KBFR+) *in vitro*. FA-targeted DM0.6K was prepared by mixing nontargeted PDC0.6K with various percentages (0, 25, 50, and 90 wt %) of targeted PDC0.6K-FA_1 (Figure S5A of the Supporting Information). Regardless of the PDC0.6K-FA_1 content, incubation of FA-targeted DMs with KBFR+ cells did not yield any noticeably enhanced cell interactions, compared to KBFR− cells used as control (Figure S5B,C of the Supporting Information). Similar results were also found when FA-targeted DMs with a longer PEG2K corona were used (data not shown). Clustered ligand arrangements of FA on the surface of DMs using PDC0.6K-FA_2 also did not result in increased targeted interactions (<1.5-fold relative to KBFR−), contrary to the results of Poon *et al.* using LDBC micelles[24] (Figure S6 of the Supporting Information). These results demonstrated that shortening of the PEG corona length did not improve the targeted cellular interactions of DMs disproving our first hypothesis. This suggested that FA was unable to bind to FR on the cell surface likely due to a combination of high PEG density near FA that resulted in decreased accessibility (steric hindrance) and reduced translational motion of FA at the surface of the DMs to initiate NP-cell surface binding.

Table 1 lists all DMs prepared in this study to reveal the effect of PEG corona chain length and content of targeted PDCs on cellular interactions of the micelles. First, to decrease the PEG density near FA and improve its translational motion, we prepared mixed micelles, which utilized a PDC with a longer PEG tether (PDC2K-FA_1) combined with nontargeted PDCs with shorter PEG coronas (either PDC0.6K or PDC1K)

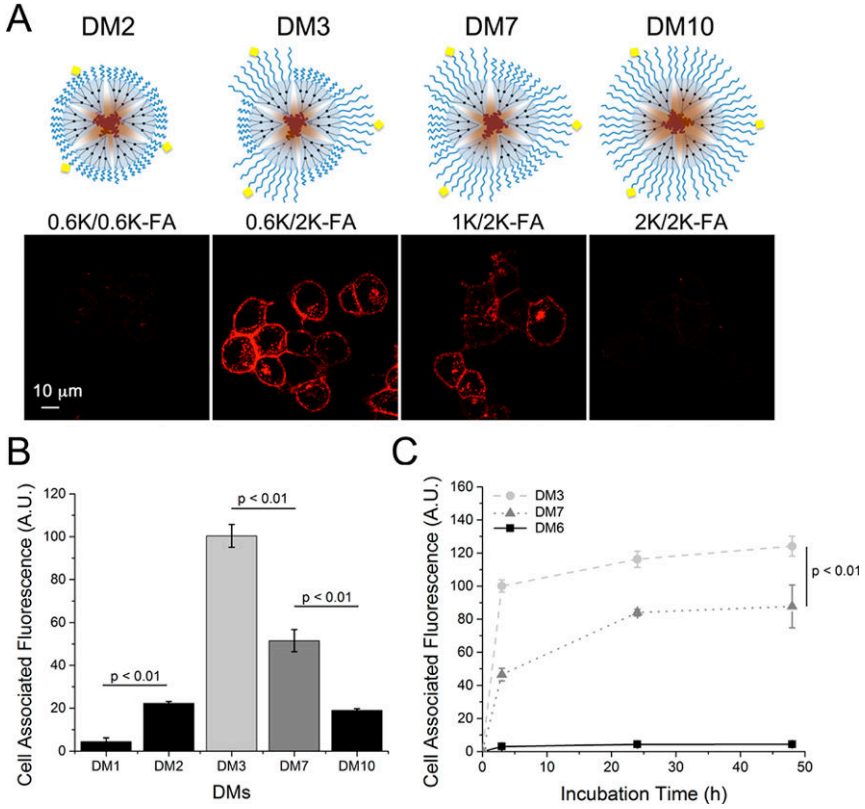


Figure 2. Effect of PEG corona length on the FA-targeted cellular interactions and interaction kinetics of DMs. Each micelle contains 5 wt % PDC2K-FA_1. Confocal microscopy images of DMs with varying PEG corona lengths (A). Quantification of DM cellular interactions by flow cytometry of various targeted DMs (B). Time-dependent FA-targeted cellular interactions of DMs, measured using flow cytometry (C).

DOI: 10.1021/acsnano.6b02708
ACS Nano 2016, 10, 6905−6914

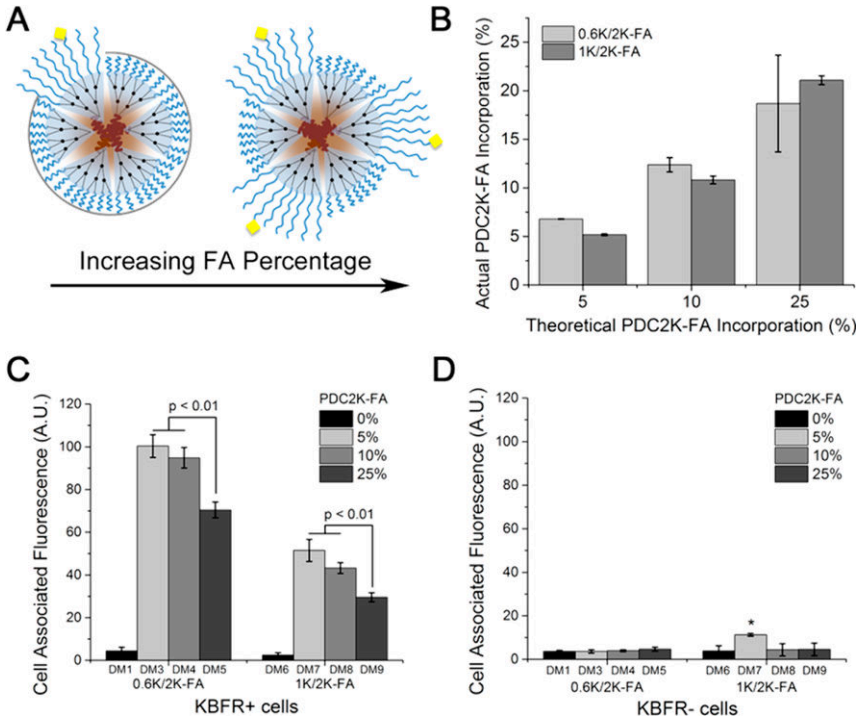


Figure 3. Incorporation of PDC2K-FA$_1$ into various DMs with different PEG corona lengths. The method used to increase FA percentage in DMs by increasing PDC2K-FA$_1$ incorporation (A). Quantification of PDC2K-FA incorporation into DMs determined using UV−vis spectroscopy (B). Quantification of cellular interactions of various targeted DMs in KBFR+ (C) and KBFR− cells (D), measured using flow cytometry.

(Figure 1ii). The cellular interactions of nontargeted DMs with various PEG corona lengths were compared to a series of FA-targeted DMs with different PEG corona lengths that incorporated 5 wt % of the PDC-FA$_1$ conjugates (denoted as DM1, 2, 3, 7, 10) (Figure 2A,B). As expected, DM2 and DM10 displayed relatively low levels of cellular interactions, whereas DM7 exhibited significantly enhanced cellular interactions over DM2 and DM10 by 2.5-fold. Shortening the PEG corona length to 0.6K using DM3 led to the most significant enhancement in cellular interactions (5-fold). Compared to nontargeted DM1 and DM6, the targeted DMs displayed cellular interactions upward of 25-fold higher (Figure 2B,C).

The differences in cellular interactions of DM3 and DM7 were found to directly influence their targeting kinetics (Figure 2C). Comparing the slopes of the curves between 0 and 3 h, DM3 and DM7 displayed significantly different rates of initial cellular association of 33.33 and 15.50 A.U./h. Following 24 h incubation, both DM3 and DM7 showed binding saturation, although DM7 was unable to reach the same level of interaction as DM3. Differences in cellular interactions among DMs could be explained by differences in cell association rate likely due to a diminished ability of FA to interact with FR when surrounded by (or embedded in) longer PEG corona at high density. Notably, the targeted cellular associations affected by the PEG corona length could have implications in solid tumor targeting and penetration, similarly to how charge and generation affect dendrimers as previously shown.[29,30]

One can argue that the observed differences could be a result of micelle disintegration in the conditions we used. To address this, we performed additional DLS studies to measure the stability of DM1, DM2, DM3, and DM10 (selected given the significant differences in terms of cell interactions as shown in Figure 2) in various solutions, such as PBS, 5× PBS, and serum-free and 10% serum containing RPMI 1640 media over 24 h. No significant size increase was found for the DMs in any of the conditions, demonstrating the high stability of the DMs (Table S2 and Figures S7−S11 of the Supporting Information).

Based on our observation indicating that the formation of targeted cellular interactions of DMs was independent of the FA content (Figure S5 of the Supporting Information), our second hypothesis was revised (Figure 1iii). Now we hypothesized that increasing the percentage of PDC2K-FA$_1$ in DM0.6K or DM1K at 5, 10, and 25 wt % (DM3, 4, 5 and 7, 8, 9, respectively) would decrease cellular interactions, since a higher percentage of PDC2K-FA$_1$ in DMs alters the ratios between longer and shorter PEG corona, resulting in the overall structure more similar to DM10 (Figure 3A). Higher percentages of PDC2K-FA$_1$ incorporation (>25 wt %) were attempted but resulted in increased nonspecific binding to the cell culture plates likely due to aggregation[22] (data not shown); therefore, those groups were not included. Up to 25 wt %, PDC2K-FA$_1$ was incorporated into DMs at ratios consistent with predefined mixing ratios (Figure 3B). Then, the cellular interactions of the various DMs were evaluated using KBFR+ and KBFR− cells (Figure 3C and D, respectively). A significant uptake of FA-targeted DMs observed for KBFR+ cells only (not for KBFR− cells), in addition to the minimal interactions of nontargeted DM1 and DM6 with KBFR+ cells, confirmed the specificity of the various FA-targeted DMs. DM4 and DM5 displayed lower levels of cellular interactions, at the 95% and 70% levels, respectively, of DM3. A more dramatic decrease in the cellular interactions was observed from DMs with PEG1K corona. For DM7, DM8, and DM9 micelles, the cellular interactions were only 47%, 43%, and 30% of the maximal interactions of DM3, respectively. It is likely that a significant reduction in targeted cellular interactions would occur at above

DOI: 10.1021/acsnano.6b02708
ACS Nano 2016, 10, 6905−6914

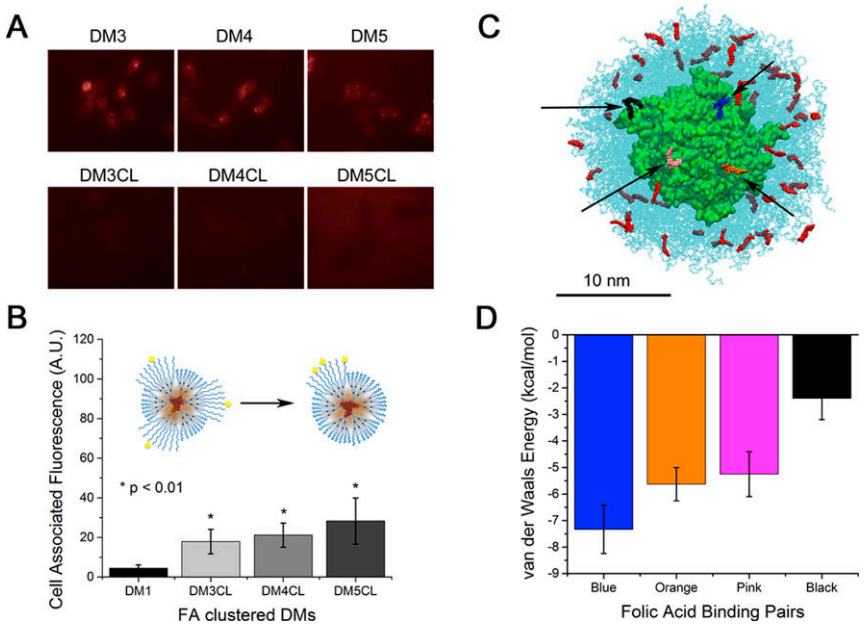


Figure 4. Effect of FA clustering on the cellular interactions of DMs. PDCs were synthesized with 3.1 FA per PDC and self-assembled into DMs. Fluorescence micrographs of unclustered (top row) and clustered (bottom row) DMs (A). Quantification of the cell associated fluorescence of clustered FA-DMs using flow cytometry (B). Data are normalized against DM3 at 100 A.U. * $p < 0.01$ indicates significant difference from corresponding unclustered DM shown in Figure 3C. MD simulation of DM0.6K-FA prepared from 60-PDC0.6K-FA$_1$ depicting intramolecular interactions between adjacent FA molecules (black arrows) (C). Note that PCL and G3 dendron are green; PEG is light blue; examples of FA binding pairs are blue, orange, pink, and black; and other FA molecules on the DM are red. Quantification of the van der Waals binding energy between various FA binding pairs present on the surface of the DM in (C) (D).

a critical percentage of PDC2K-FA$_1$ (5% as seen for DM3) incorporation particularly when the PEG tether length with FA is not sufficiently longer than the length of the PEG corona (Figure S5 of the Supporting Information). This indicates that the nontargeted PEG corona length is a governing factor for determining the cellular interactions of FA-targeted DMs. These results support our revised hypothesis that an increase in the percentage of PDC2K-FA$_1$ in DMs to above a critical level diminishes targeted cellular interactions of DMs.

In a similar manner to our second hypothesis, we assessed our third hypothesis that ligand clustering on the surface of DMs would facilitate the formation of multivalent interactions and subsequently enhance cellular interactions (Figure 1iv). FA-targeted PDC2K was synthesized to have approximately 3.1 FA per PDC (denoted PDC2K-FA$_3$) (Table S1 and Figures S2−S3 of the Supporting Information). Clustered (CL) DMs (noted as DM3−5CL) were prepared at similar FA contents as DM3−5. In sharp contrast to a previous report by the Hammond group suggesting the benefits of FA-clustering on LDBC micelles,[24] the cellular interactions of clustered DMs were significantly decreased (by up to 6 times) compared to unclustered DMs (Figure 4A,B). These results disproved our third hypothesis that the clustered arrangement of FA on the surface of DMs would promote the formation of enhanced cellular interactions.

To better understand the reasons underlying the diminished cellular interactions due to FA clustering, the size, surface area, and aggregation number (N_{agg}) for generation 5 (G5) polyamidoamine (PAMAM) dendrimers (5 nm, 79 nm^2, 1)[22,31] and LDBC micelles (90 nm, 25447 nm^2, 1000)[24] were compared to DMs (20 nm, 1256 nm^2, 60) using previously reported values (Table S3). We have calculated the surface area occupied by a single FA molecule, which is required to achieve the most significant enhancement in FA-mediated cellular interactions.[22,24,31] Approximately 5 FA molecules per G5 dendrimer and 3 FA per LDBC resulted in the most significant enhancement in cellular interactions, which corresponded to 16 and 8 nm^2 of the surface area per FA, respectively. Increased FA density (decreased surface area per FA) resulted in diminished cellular interactions. In our study, PDC2K-FA was prepared with either 1 or 3 FA molecules, which corresponded to a surface area per FA of 21 or 7 nm^2, respectively. Since the surface area per FA for PDC2K-FA$_3$ was less than the surface area per FA for G5 dendrimer or LDBC micelles (*i.e.*, 7 vs 16 or 8 nm^2), it is possible that FA may interact intermolecularly with other FA in close proximity (Figure 4C). At a high FA density on the surface of DMs, majorities of surface-bound FA were found as dimers. Four FA binding pairs are colored and indicated by black arrows as examples, although many other binding pairs are clearly observed. The van der Waals (vdW) energy between those four different FA pairs on the surface of DM0.6K was measured between −2 and −8 kcal/mol, confirming intermolecular interactions between neighboring FA (Figure 4D). Noninteracting FA molecules on the surface of DMS have a vdW energy of 0 kcal/mol. Considering that the binding pocket of FR is only large enough to accommodate a single FA,[32] the formation of intermolecular interactions between adjacent FA supports our experimental findings that clustering of FA on the surface of DMs lead to diminished cellular interactions.

To obtain a molecular-level understanding of the factors that contribute to the formation of FA-targeted DMs−cellular interactions, we modeled the DMs by atomistic MD simulations. We selected seven FA-targeted DMs (Figure S12 of the Supporting Information) that represented the experimentally evaluated DMs. DMs that were simulated (S)

DOI: 10.1021/acsnano.6b02708
ACS Nano 2016, 10, 6905−6914

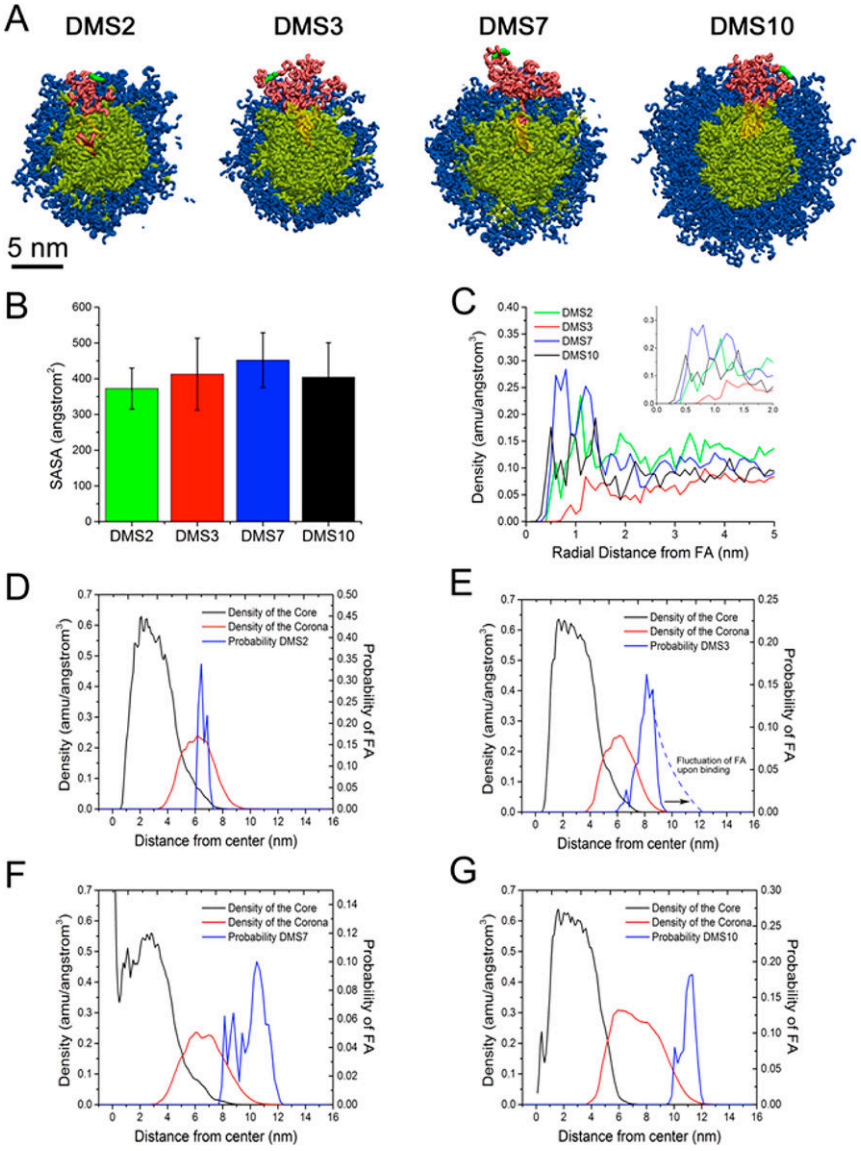


Figure 5. MD simulation of the effect of PEG corona lengths on spreading of PEG chains, PEG density, SASA, and probability distribution of the position of FA. Cross sections of DMS displaying the core (yellow), PEG chains (blue), PDC-FA$_1$ (pink), FA (green) (A). Water is not shown for clarity. SASA of various DMS formulations (B). Density distribution of atoms surrounding FA on the surface of DMS (C). Inset: density distribution from 0 to 2 nm. Probability distribution of the position of FA from the surface of the DMS2, 3, 7, and 10 (D−G). SASA, density, and probability distribution of the position of FA are the data calculated over 500, 100, and 500 frames, respectively.

corresponded to the experimentally tested DMs (*e.g.*, DM3 = DMS3). Individual PDCs were prepared using visual molecular dynamics (VMD) and arranged into spherical assemblies forming DMS that consisted of N_{agg} of 60. The size of each DMS modeled was calculated using VMD (Table S4 of the Supporting Information) and was similar to those measured by DLS (Table 1).

We then investigated the DMS structure and dynamics by analyzing the solvent accessible surface area (SASA) of FA, the local PEG density near FA, and the distribution of FA positions with respect to the micelle center (see Supporting Information for additional details). In Figure 5A, it is clearly shown from the MD simulation cross sections of DMS that the PEG corona length influenced the amount of spreading of the PEG chains of the FA-targeted PDCs (pink color). DMS with the same PEG corona length as the targeted PEG length displayed more condensed and restricted conformations, whereas DMS with PEG coronas shorter than the targeted PDC PEG length displayed more relaxed and flexible conformations. Without optimization of the chain length of the PEG-targeting ligand conjugates, FA could become buried within the core, as shown for PEG-poly(lactide-*co*-glycolide) (PLGA) NPs.[33]

Assuming that the availability of FAs is critical for targeted cellular interactions of DMs, we calculated the SASA of FA on DMS to show how much of its surface is covered by water. Interestingly, the SASA results for the selected FA-targeted DMS with different PEG corona lengths did not yield significant differences, suggesting that SASA of FA is not completely responsible for determining the targeting capability of FA-targeted DMs (Figure 5B and Figure S13A of the Supporting Information). SASA cannot fully explain the limited targeted cellular interactions of DM2 and DM10, which both have relatively large SASA.

DOI: 10.1021/acsnano.6b02708
ACS Nano 2016, 10, 6905−6914

To provide further understanding of how the PEG corona length affected the cellular interactions of FA-targeted DMs, we calculated the atomic density distribution around FA with 1 Å resolution (Figure 5C). However, this density also correlated only partially with the level of FA-targeted DM cellular interactions. DMS3 displayed the lowest PEG density (<0.05 amu/Å^3) within 1 nm of FA, which could be attributed to the large difference between PEG2K-FA$_1$ and the PEG0.6K corona chain molecular weights and the associated high level of PEG2K spreading. The PEG densities around FA for DMS2, DMS7, and DMS10 were higher than for DMS3, but contrary to level of FA-targeted DM cellular interactions, the PEG densities were only moderately different one from another and reached a maximum of 0.3 amu/Å^3. Similar densities were also observed for DMs with PEG0.6K coronas and increasing percentages of PDC2K-FA$_1$ incorporation (Figure S13B of the Supporting Information). Although these results supported the strong cellular interactions of DM3, the density of DMS7 was much greater than DMS3, suggesting that an additional factor is influencing FA-targeting of DMs.

Finally, we explored the FA availability (position) above the PEG corona, assuming that the free availability of FA-targeting ligand could be important for the initiation of selective ligand−receptor interactions.[34] Figure 5D−G presents an overlay of the hydrophobic core density (black line), the PEG corona density (red line), and the probability distribution of FA from the DM center (blue line) for DMS2, DMS3, DMS7, and DMS10, respectively. On average, the density of the core reached 0.6 amu/Å^3 for all DMS. DMS10 displayed the most compact core (radius of 6 nm), while other cores radii ranged from 7 to 9 nm. The thickness of each PEG corona layer correlated well with the PEG chain length.

On the surface of DMS2, FA was mostly hidden within the PEG corona (Figure 5D). On DMS7 and DMS10, the DMs and PEG-FA chains were on average of similar lengths, so FA could fluctuate to its near full extension while being close to the surface (Figure 5F,G). FA is more freely available on DMS7 than on DMS10, which agrees with the observed FA activities of these two DMs *in vitro*. However, FA was never found fully extended above the surface of DMS3, since most of the time it is close to the short PEG corona interface (Figure 5E). Therefore, DMS3 may be able to provide more conformational freedom compared to the other micelles (dotted line in Figure 5E). This can be an important factor for the FA binding to FR. In the presence of a nearby FR, the FA distributions might reach up to FR, as long as the DMs provide enough conformational space (DMS3). FR is considered to have a deep binding pocket,[32] where the pterin ring of FA forms hydrogen bonds with amino acids within the protein. The depth of the receptor-binding pocket determines the size of spatial FA fluctuations (beyond the PEG corona), which are necessary for FA to optimally reach the binding site. For example, virtually all the RGD binding sites can be reached with peptides extending 46 Å from the surface of polyacrylonitrile beads.[35] However, the binding pocket of integrin receptor head is as deep as 80 Å.

CONCLUSION

Taken together, our results demonstrate a high level of controllability over the formation of FA-targeted cellular interactions of DMs through modulation of the PEG corona length and the percentage of PDC-FA incorporation. The greatest enhancement in targeted cellular interactions (>25-fold) was observed for DM3 that consisted of 95 wt % nontargeted PDC0.6K-Ac and 5 wt % targeted PDC2K-FA$_1$. Further increased percentages (above 5 wt %) of PDC2K-FA$_1$ incorporated into DMs led to reductions in targeted cellular interactions. To understand these observations, we performed atomistic MD simulations and quantitatively assessed three parameters related to the FA ligands (SASA, local PEG density, and the position distribution of FA). These results provide strong evidence that the ability of FA to depart from the surface of DMs to facilitate the initial cell surface binding interaction is a critical contributor for determining FA-mediated cellular interactions of DMs. Larger FA fluctuations are related to a lower PEG density surrounding the targeting ligand, which is also observed to correlate with the strength of cellular interactions. Additionally, we anticipate that the coiled state of the longer PEG chains surrounding the targeting ligand due to the dendritic architecture may be useful to reduce the negative effects of the protein corona on targeted NP cellular interactions by reducing the relative amounts of serum protein adsorption into PEG chains.[36−38] We anticipate that the concepts and considerations presented herein using DMs will be widely applicable toward future avidity-targeted NP development by providing a series of cues to design effective NPs as nanocarriers for the treatment of various diseases.

METHODS

Materials. Dicyclohexylcarbodiimide (DCC), *N*-hydroxysuccinimide (NHS), and FA were purchased from Sigma-Aldrich Co. (St. Louis, U.S.A.). Regenerated cellulose dialysis membrane was purchased from Spectrum Laboratories (CA, U.S.A.). All solvents and reagents were used without further purification unless otherwise specified.

Synthesis of Nontargeted PDCs and Rhodamine (Rho)-Labeled PDCs. PDCs used in this study were synthesized using similar protocol to those previously described starting from PCL3.5K-G3-PNP.[18−20]

Synthesis of FA)-Targeted PDCs (PDC-FA). FA-targeted PDCs were synthesized by coupling PCL-G3-PEG(0.6K or 2K)-NH$_2$ (PDC-NH$_2$) to an NHS-activated FA. First, FA was activated with DCC and NHS as described previously.[39] Briefly, FA (50 mg, 0.113 mmol) was dissolved in 1.5 mL dimethyl sulfoxide (DMSO). DCC (25 mg, 0.121 mmol) dissolved in 0.5 mL DMSO followed by NHS (44.85 mg, 0.390 mmol) dissolved in 0.5 mL DMSO were then added dropwise to the FA solution and stirred overnight. The dicyclohexylurea byproduct was then filtered off using a 0.2 μm nylon syringe filter to yield the NHS-activated FA solution at a concentration of 20 mg/mL. The solution was then used immediately.

Synthesis of PDC0.6K-FA$_1$ and PDC0.6K-FA$_3$. NHS-activated FA solution (2.97 mg, 0.00674 mmol, 2 equiv, 148.7 μL of stock solution for PDC0.6K-FA$_1$ or 5.95 mg, 0.0135 mmol, 4 equiv, 297.5 μL of stock solution for PDC0.6K-FA$_2$) in 0.5 mL DMSO was added dropwise to a stirring solution of PDC0.6K-NH$_2$ (25 mg, 0.0034 mmol, 7418.79 Da from ^{1}H NMR) in DMSO (2 mL). The reaction was performed at room temperature for 24 h. To the stirring solution, triethylamine (32.74 mg, 0.324 mmol, 45.09 μL, 20% excess to acetic anhydride) was added. Acetic anhydride (27.52 mg, 0.270 mmol, 25.48 μL) was then added dropwise to the stirring solution. The reaction was allowed to progress for 24 h at room temperature. The solution was then dialyzed against dH$_2$O for 24 h using a 3.5 kDa MWCO membrane and lyophilized for 2 days.

Synthesis of PDC2K-FA$_1$. NHS-activated FA solution (1.51 mg, 0.0034 mmol, 2 equiv, 75.6 μL of stock solution) in 0.5 mL DMSO was added dropwise to a stirring solution of PDC2K-NH$_2$ (25 mg, 0.0017 mmol, 14596.3 Da from ^{1}H NMR) in 2 mL DMSO. The reaction was performed at room temperature for 24 h. To the stirring solution, triethylamine (16.6 mg, 0.164 mmol, 22.92 μL, 20% excess to acetic anhydride) was added. Acetic anhydride (14.0 mg, 0.137 mmol, 12.95 μL) was then added dropwise to the stirring solution. The

DOI: 10.1021/acsnano.6b02708
ACS Nano 2016, 10, 6905−6914

reaction was allowed to proceed for 24 h at room temperature. The solution was then dialyzed against dH_2O for 24 h using a 3.5 kDa MWCO membrane and lyophilized for 2 days.

Synthesis of PDC2K-FA$_3$. NHS-activated FA solution (1.86 mg, 0.0042 mmol, 5 equiv, 93 μL of stock solution) in 0.5 mL DMSO was added dropwise to a stirring solution of PDC2K-NH_2 (12 mg, 0.00084 mmol, 14 238 Da from NMR) in DMSO (1.5 mL). The reaction was performed at room temperature for 24 h. The solution was then dialyzed against dH_2O for 24 h using a 3.5 kDa MWCO membrane and lyophilized for 2 days.

PDC and DM Characterization. ^{1}H NMR spectra were recorded at 400 MHz (DPX-400 NMR spectrometer, Bruker Biospin Co., MA, U.S.A.). NMR chemical shifts are reported in ppm with calibration against a solvent signal (7.24 ppm for $CDCl_3$ and 2.5 ppm for DMSO-d_6). GPC measurements were carried out using a 600 HPLC pump, 717plus Autosampler, and a 2414 refractive index detector (Waters, Milford, MA, U.S.A.) using THF as the mobile phase at 0.5 mL/min with Waters Styragel HR2 and HR4E columns at 30 °C. Molecular weight (M_n) was determined relative to the elution volume of polystyrene standards.

DLS and ζ Potential Analysis. Particle size of the various DMs (1 mg/mL) was measured using a NICOMP 380 ζ potential/particle sizer (Particle Sizing Systems, Santa Barbara, CA) as previously described.[18] For experiments evaluating the stability of DMs in PBS, 5× PBS, and serum-free and 10% fetal bovine serum (FBS) containing RPMI 1640 media over 24 h, the particle size was measured using a Malvern Zetasizer ZS (Malvern Instruments, Westborough, MA) at concentrations of 0.5 mg/mL.[38] All measurements were performed in triplicate in ddH_2O (pH 5.6) using unfiltered micelle samples.

Micelle Preparation. DMs with varying content of FA were prepared using the dialysis method. Briefly, individual PDCs (Figure S2 of the Supporting Information) were combined together in 250 μL DMF and stirred for 5−10 min. To the stirring solution, 200 μL of dH_2O was then added dropwise to induce the self-assembly of the DMs. The solution was allowed to stir for at least 10 min before being placed into a 3.5 kDa MWCO dialysis membrane and dialyzing against dH_2O overnight to remove the organic solvent. The following day, the micelle solution was then collected and centrifuged for 5 min at to 9300 × g to remove any aggregates, and the supernatant was collected. The final micelle solution was diluted to 1 mL with dH_2O (1 mg/mL) and subjected to further characterization using fluorescence spectroscopy and DLS/ZP. PDC0.6K-Rho-Ac was incorporated into the DMs at 10 wt % for visualization.[20]

Cell Culture. KB cells (human oral carcinoma cells) were obtained from American Type Culture Collection (ATCC) (Manassas, VA, U.S.A.) and grown continuously as a monolayer in 75 cm^2 T flasks in GIBCO RPMI 1640 medium (Invitrogen Corporation, Carlsbad, CA, U.S.A.) in a humidified incubator at 37 °C and 5% CO_2. RPMI was supplemented with penicillin (100 units/ml), streptomycin, and 10% heat-inactivated FBS (Invitrogen Corporation, Carlsbad, CA, U.S.A.) before use.

Cellular Uptake of DMs. For confocal laser scanning microscope (CLSM) observation, KB cells were seeded in glass bottom culture dishes (Corning) or 8-well Millicell EZ slides (Millipore, MN) at densities of 2 × 10^5 and 1 × 10^5 cells/well, respectively. The cells were allowed to adhere for overnight before starting the experiments. Prior to the experiment, the fluorescence intensity of DM samples was measured and normalized. This enabled direct differences in cellular interactions to be compared between groups.

Cells were then treated with 60 μg/mL of Rho-labeled DMs in serum free RPMI or DPBS to assess any potential differences in internalization depending on PEG corona length, PDC-FA percent incorporation, or FA clustering. After incubation, the wells were washed two times with 1× DPBS and fixed with a 4% paraformaldehyde solution and mounting agent with DAPI. The specimens were visualized using a Carl Zeiss microscope (LSM 710, Carl Zeiss MicroImaging GmbH, Gena, Germany), and images were obtained using a 40× objective (Objective "C-Apochromat" 40×/1.20 W corr, Carl Zeiss MicroImaging GmbH, Gena, Germany). Zen (Carl Zeiss MicroImaging GmbH, Gena, Germany) was used for processing of images.

Cellular Association of Surface-Modified DMs by Flow Cytometry. For flow cytometry measurement, KB cells were seeded in 12-well plates at a density of 2 × 10^5 cells/well 24 h prior to the experiment to allow for cell adherence. Cells were then treated with 1 mL of 60 μg/mL of FA-targeted DM solutions in DPBS or serum free RPMI for a specified amount of time. After incubation, the cells were washed twice with 1 mL of 1× DPBS and suspended by 300 μL trypsin/EDTA. The resultant cell suspensions were then centrifuged at 500 × g for 5 min, the supernatant was discarded, and the cells were resuspended in 500 μL of a 1% paraformaldehyde solution and transferred to flow cytometry sample tubes. Samples were examined using a LSR Fortessa flow cytometer (Beckman Coulter, Franklin Lakes, NJ).

MD Simulations of DMs. Atomistic MD simulations of FA-targeted DM assemblies with aggregation numbers, N_{agg}, of 60 were performed in 150 mM NaCl solution. We used the NAMD package[40] and the CHARMM force field (CHARMM27, C35r revision for ethers, and general force field)[41−43] for simulation. In the simulations, we used Langevin dynamics with damping constant of γ_{Lang} = 0.1 ps^{-1} to achieve a faster relaxation. Nonbonded interactions were calculated using the cutoff distance of d = 10 Å. Long-range electrostatic interactions were calculated by the PME method,[44] and the MD integration time step was set to 2 fs. The individual PDCs were equilibrated for ∼25 ns in water, using the NPT ensemble with periodic boundary conditions applied (P = 1 bar and T = 300 K). We visualized all the PDCs using VMD1.9.[45]

SASA. We calculated SASA using VMD plugin. In this calculation, the radius of the solvent was 1.4 Å. The solvent radius was added to the vdWs radius of each atom. Then a sphere of the combined radius was imaged. 500 points were randomly distributed on the surface of the sphere. All the points were checked against the surface of all the neighboring atoms. The accessible number of points was multiplied with the assigned surface area each point represents. Here we initially selected the FA in the whole micelle. Then we calculated the exposure of the FA toward the solvent. In case of multiple FAs, we calculated the average over the number of FAs. We performed the analysis over 500 frames during 5 ns.

Atomic Density Calculation. We calculated the radial density distribution of the hydrophobic core and PEGylated corona of each micelle. We also separately calculated the atomic density distribution surrounding the FA. The densities $[\rho(r)]$ were calculated using the equation:

$$\rho(r) = \frac{1}{N_t}\sum_{t=1}^{N_t}\sum_{i=1}^{N_a}\frac{m_i}{V}$$

where m_i is the mass of ith atom within the set of N_a atoms found in the bin with volume V. Each bin is a spherical shell with thickness Δr = 1 Å. For the case of core and the corona, the concentric spheres were centered at the center of the micelle. For the atomic density distribution surrounding the FA, the shells were centered at the center of the FA. In case of multiple FAs, we calculated the average over the number of FAs. The density calculations were performed over N_t = 100 frames during 1 ns of simulation.

Distribution of the Position of FA. We calculated the distance of the FA from the center of the micelle for each frame. Using this data, we prepared a histogram to show the distance distribution of the FA from the center of the micelle. The histogram bin size is 2 Å. We measured the distance for 500 frames during 5 ns. We normalized the number of frames in each bin by the total number of frames.

ASSOCIATED CONTENT

Supporting Information

The Supporting Information is available free of charge on the ACS Publications website at DOI: 10.1021/acsnano.6b02708.

^{1}H NMR and GPC characterization of PDC polymers, DLS and ζ potential plots, surface area calculations,

DOI: 10.1021/acsnano.6b02708
ACS Nano 2016, 10, 6905−6914

VMD measured diameters, synthesis scheme for PDC-FA polymers, schematic of PDC library generated, microscopy images and flow cytometry quantitation of DM cellular interactions, representation of various DMs modeled by MD simulations (PDF)

AUTHOR INFORMATION

Corresponding Author

*E-mail: sphong@uic.edu.

Notes

The authors declare no competing financial interest.

ACKNOWLEDGMENTS

This study was supported by the Hans W. Vahlteich Research Fund from the University of Illinois at Chicago (UIC), NCI/NIH (grant no. 1R01CA182528), NSF (grant no. DMR-1409161), Alex's Lemonade Stand Foundation for Childhood Cancer, and Leukemia & Lymphoma Society. The MD simulation work was supported by NSF (grant no. DMR-1309765) and the UIC−LAS Award for Faculty in the Sciences. The research was conducted in a facility constructed with support from the NIH (grant C06RR15482). R.M.P. was partially supported by the Dean's Scholarship from UIC. M.G. was supported by LASURI and the support from the Camille and Henry Dreyfus Foundation through the Senior Scientist Mentor Award to Prof. Cynthia J. Jameson.

REFERENCES

(1) Peer, D.; Karp, J. M.; Hong, S.; Farokhzad, O. C.; Margalit, R.; Langer, R. Nanocarriers as an Emerging Platform for Cancer Therapy. *Nat. Nanotechnol.* **2007**, *2*, 751−760.

(2) Pearson, R. M.; Sunoqrot, S.; Hsu, H.-j.; Bae, J. W.; Hong, S. Dendritic Nanoparticles: The Next Generation of Nanocarriers? *Ther. Delivery* **2012**, *3*, 941−959.

(3) Pearson, R. M.; Hsu, H.-j.; Bugno, J.; Hong, S. Understanding Nano-Bio Interactions to Improve Nanocarriers for Drug Delivery. *MRS Bull.* **2014**, *39*, 227−237.

(4) Owens, D. E., III; Peppas, N. A. Opsonization, Biodistribution, and Pharmacokinetics of Polymeric Nanoparticles. *Int. J. Pharm.* **2006**, *307*, 93−102.

(5) Walkey, C. D.; Olsen, J. B.; Guo, H.; Emili, A.; Chan, W. C. W. Nanoparticle Size and Surface Chemistry Determine Serum Protein Adsorption and Macrophage Uptake. *J. Am. Chem. Soc.* **2012**, *134*, 2139−2147.

(6) Perry, J. L.; Reuter, K. G.; Kai, M. P.; Herlihy, K. P.; Jones, S. W.; Luft, J. C.; Napier, M.; Bear, J. E.; DeSimone, J. M. Pegylated Print Nanoparticles: The Impact of Peg Density on Protein Binding, Macrophage Association, Biodistribution, and Pharmacokinetics. *Nano Lett.* **2012**, *12*, 5304−5310.

(7) Pearson, R. M.; Juettner, V.; Hong, S. Biomolecular Corona on Nanoparticles: A Survey of Recent Literature and Its Implications in Targeted Drug Delivery. *Front. Chem.* **2014**, *2*.10.3389/fchem.2014.00108

(8) Byrne, J. D.; Betancourt, T.; Brannon-Peppas, L. Active Targeting Schemes for Nanoparticle Systems in Cancer Therapeutics. *Adv. Drug Delivery Rev.* **2008**, *60*, 1615−1626.

(9) Davis, M. E.; Chen, Z.; Shin, D. M. Nanoparticle Therapeutics: An Emerging Treatment Modality for Cancer. *Nat. Rev. Drug Discovery* **2008**, *7*, 771−782.

(10) Gabizon, A.; Horowitz, A. T.; Goren, D.; Tzemach, D.; Mandelbaum-Shavit, F.; Qazen, M. M.; Zalipsky, S. Targeting Folate Receptor with Folate Linked to Extremities of Poly(Ethylene Glycol)-Grafted Liposomes: *In Vitro* Studies. *Bioconjugate Chem.* **1999**, *10*, 289−298.

(11) Hak, S.; Helgesen, E.; Hektoen, H. H.; Huuse, E. M.; Jarzyna, P. A.; Mulder, W. J. M.; Haraldseth, O.; Davies, C. d. L. The Effect of Nanoparticle Polyethylene Glycol Surface Density on Ligand-Directed Tumor Targeting Studied *in Vivo* by Dual Modality Imaging. *ACS Nano* **2012**, *6*, 5648−5658.

(12) Stefanick, J. F.; Ashley, J. D.; Kiziltepe, T.; Bilgicer, B. A Systematic Analysis of Peptide Linker Length and Liposomal Polyethylene Glycol Coating on Cellular Uptake of Peptide-Targeted Liposomes. *ACS Nano* **2013**, *7*, 2935−2947.

(13) Sawant, R. R.; Sawant, R. M.; Kale, A. A.; Torchilin, V. P. The Architecture of Ligand Attachment to Nanocarriers Controls Their Specific Interaction with Target Cells. *J. Drug Target* **2008**, *16*, 596−600.

(14) Lee, R. J.; Low, P. S. Delivery of Liposomes into Cultured Kb Cells *Via* Folate Receptor-Mediated Endocytosis. *J. Biol. Chem.* **1994**, *269*, 3198−3204.

(15) Gabizon, A.; Shmeeda, H.; Horowitz, A. T.; Zalipsky, S. Tumor Cell Targeting of Liposome-Entrapped Drugs with Phospholipid-Anchored Folic Acid−Peg Conjugates. *Adv. Drug Delivery Rev.* **2004**, *56*, 1177−1192.

(16) Yamada, A.; Taniguchi, Y.; Kawano, K.; Honda, T.; Hattori, Y.; Maitani, Y. Design of Folate-Linked Liposomal Doxorubicin to Its Antitumor Effect in Mice. *Clin. Cancer Res.* **2008**, *14*, 8161−8168.

(17) Stefanick, J. F.; Ashley, J. D.; Bilgicer, B. Enhanced Cellular Uptake of Peptide-Targeted Nanoparticles through Increased Peptide Hydrophilicity and Optimized Ethylene Glycol Peptide-Linker Length. *ACS Nano* **2013**, *7*, 8115−8127.

(18) Bae, J. W.; Pearson, R. M.; Patra, N.; Sunoqrot, S.; Vukovic, L.; Kral, P.; Hong, S. Dendron-Mediated Self-Assembly of Highly Pegylated Block Copolymers: A Modular Nanocarrier Platform. *Chem. Commun.* **2011**, *47*, 10302−10304.

(19) Pearson, R. M.; Patra, N.; Hsu, H.-j.; Uddin, S.; Kral, P.; Hong, S. Positively Charged Dendron Micelles Display Negligible Cellular Interactions. *ACS Macro Lett.* **2013**, *2*, 77−81.

(20) Hsu, H.-j.; Sen, S.; Pearson, R. M.; Uddin, S.; Král, P.; Hong, S. Poly(Ethylene Glycol) Corona Chain Length Controls End-Group-Dependent Cell Interactions of Dendron Micelles. *Macromolecules* **2014**, *47*, 6911−6918.

(21) del Pino, P.; Yang, F.; Pelaz, B.; Zhang, Q.; Kantner, K.; Hartmann, R.; Martinez de Baroja, N.; Gallego, M.; Möller, M.; Manshian, B. B.; Soenen, S. J.; Riedel, R.; Hampp, N.; Parak, W. J. Basic Physicochemical Properties of Polyethylene Glycol Coated Gold Nanoparticles That Determine Their Interaction with Cells. *Angew. Chem., Int. Ed.* **2016**, *55*, 5483−5487.

(22) Hong, S.; Leroueil, P. R.; Majoros, I. n. J.; Orr, B. G.; Baker, J. R.; Banaszak Holl, M. M. The Binding Avidity of a Nanoparticle-Based Multivalent Targeted Drug Delivery Platform. *Chem. Biol.* **2007**, *14*, 107−115.

(23) Myung, J. H.; Gajjar, K. A.; Saric, J.; Eddington, D. T.; Hong, S. Dendrimer-Mediated Multivalent Binding for the Enhanced Capture of Tumor Cells. *Angew. Chem., Int. Ed.* **2011**, *50*, 11769−11772.

(24) Poon, Z.; Chen, S.; Engler, A. C.; Lee, H.-i.; Atas, E.; von Maltzahn, G.; Bhatia, S. N.; Hammond, P. T. Ligand-Clustered "Patchy" Nanoparticles for Modulated Cellular Uptake and *in Vivo* Tumor Targeting. *Angew. Chem., Int. Ed.* **2010**, *49*, 7266−7270.

(25) Ross, J. F.; Chaudhuri, P. K.; Ratnam, M. Differential Regulation of Folate Receptor Isoforms in Normal and Malignant Tissues *in Vivo* and in Established Cell Lines. Physiologic and Clinical Implications. *Cancer* **1994**, *73*, 2432−2443.

(26) Weitman, S. D.; Lark, R. H.; Coney, L. R.; Fort, D. W.; Frasca, V.; Zurawski, V. R.; Kamen, B. A. Distribution of the Folate Receptor Gp38 in Normal and Malignant Cell Lines and Tissues. *Cancer Res.* **1992**, *52*, 3396−3401.

(27) Sudimack, J.; Lee, R. J. Targeted Drug Delivery *Via* the Folate Receptor. *Adv. Drug Delivery Rev.* **2000**, *41*, 147−162.

(28) Sunoqrot, S.; Bae, J. W.; Pearson, R. M.; Shyu, K.; Liu, Y.; Kim, D.-H.; Hong, S. Temporal Control over Cellular Targeting through Hybridization of Folate-Targeted Dendrimers and Peg-Pla Nanoparticles. *Biomacromolecules* **2012**, *13*, 1223−1230.

DOI: 10.1021/acsnano.6b02708
ACS Nano 2016, 10, 6905−6914

(29) Sunoqrot, S.; Liu, Y.; Kim, D.-H.; Hong, S. *In Vitro* Evaluation of Dendrimer−Polymer Hybrid Nanoparticles on Their Controlled Cellular Targeting Kinetics. *Mol. Pharmaceutics* **2013**, *10*, 2157−2166.
(30) Bugno, J.; Hsu, H. J.; Pearson, R. M.; Noh, H.; Hong, S., Size and Surface Charge of Engineered Poly(Amidoamine) Dendrimers Modulate Tumor Accumulation and Penetration: A Model Study Using Multicellular Tumor Spheroids. *Mol. Pharmaceutics* **2016**, Article ASAP.10.1021/acs.molpharmaceut.5b00946
(31) van Dongen, M. A.; Silpe, J. E.; Dougherty, C. A.; Kanduluru, A. K.; Choi, S. K.; Orr, B. G.; Low, P. S.; Banaszak Holl, M. M. Avidity Mechanism of Dendrimer−Folic Acid Conjugates. *Mol. Pharmaceutics* **2014**, *11*, 1696−1706.
(32) Chen, C.; Ke, J.; Zhou, X. E.; Yi, W.; Brunzelle, J. S.; Li, J.; Yong, E.-L.; Xu, H. E.; Melcher, K. Structural Basis for Molecular Recognition of Folic Acid by Folate Receptors. *Nature* **2013**, *500*, 486−489.
(33) Valencia, P. M.; Hanewich-Hollatz, M. H.; Gao, W.; Karim, F.; Langer, R.; Karnik, R.; Farokhzad, O. C. Effects of Ligands with Different Water Solubilities on Self-Assembly and Properties of Targeted Nanoparticles. *Biomaterials* **2011**, *32*, 6226−6233.
(34) Wong, J. Y.; Kuhl, T. L.; Israelachvili, J. N.; Mullah, N.; Zalipsky, S. Direct Measurement of a Tethered Ligand-Receptor Interaction Potential. *Science* **1997**, *275*, 820−822.
(35) Beer, J. H.; Springer, K. T.; Coller, B. S. Immobilized Arg-Gly-Asp (Rgd) Peptides of Varying Lengths as Structural Probes of the Platelet Glycoprotein Iib/Iiia Receptor. *Blood* **1992**, *79*, 117−128.
(36) Salvati, A.; Pitek, A. S.; Monopoli, M. P.; Prapainop, K.; Bombelli, F. B.; Hristov, D. R.; Kelly, P. M.; Aberg, C.; Mahon, E.; Dawson, K. A. Transferrin-Functionalized Nanoparticles Lose Their Targeting Capabilities When a Biomolecule Corona Adsorbs on the Surface. *Nat. Nanotechnol.* **2013**, *8*, 137−143.
(37) Dai, Q.; Walkey, C.; Chan, W. C. W. Polyethylene Glycol Backfilling Mitigates the Negative Impact of the Protein Corona on Nanoparticle Cell Targeting. *Angew. Chem., Int. Ed.* **2014**, *53*, 5093−5096.
(38) Pelaz, B.; del Pino, P.; Maffre, P.; Hartmann, R.; Gallego, M.; Rivera-Fernández, S.; de la Fuente, J. M.; Nienhaus, G. U.; Parak, W. J. Surface Functionalization of Nanoparticles with Polyethylene Glycol: Effects on Protein Adsorption and Cellular Uptake. *ACS Nano* **2015**, *9*, 6996−7008.
(39) Yang, X.; Deng, W.; Fu, L.; Blanco, E.; Gao, J.; Quan, D.; Shuai, X. Folate-Functionalized Polymeric Micelles for Tumor Targeted Delivery of a Potent Multidrug-Resistance Modulator Fg020326. *J. Biomed. Mater. Res., Part A* **2008**, *86A*, 48−60.
(40) Phillips, J. C.; Braun, R.; Wang, W.; Gumbart, J.; Tajkhorshid, E.; Villa, E.; Chipot, C.; Skeel, R. D.; Kalé, L.; Schulten, K. Scalable Molecular Dynamics with Namd. *J. Comput. Chem.* **2005**, *26*, 1781−1802.
(41) MacKerell, A. D.; Bashford, D.; Bellott, M.; Dunbrack, R. L.; Evanseck, J. D.; Field, M. J.; Fischer, S.; Gao, J.; Guo, H.; Ha, S.; Joseph-McCarthy, D.; Kuchnir, L.; Kuczera, K.; Lau, F. T. K.; Mattos, C.; Michnick, S.; Ngo, T.; Nguyen, D. T.; Prodhom, B.; Reiher, W. E.; Roux, B.; Schlenkrich, M.; Smith, J. C.; Stote, R.; Straub, J.; Watanabe, M.; Wiorkiewicz-Kuczera, J.; Yin, D.; Karplus, M. All-Atom Empirical Potential for Molecular Modeling and Dynamics Studies of Proteins. *J. Phys. Chem. B* **1998**, *102*, 3586−3616.
(42) Lee, H.; Venable, R. M.; MacKerell, A. D.; Pastor, R. W. Molecular Dynamics Studies of Polyethylene Oxide and Polyethylene Glycol: Hydrodynamic Radius and Shape Anisotropy. *Biophys. J.* **2008**, *95*, 1590−1599.
(43) Vanommeslaeghe, K.; Hatcher, E.; Acharya, C.; Kundu, S.; Zhong, S.; Shim, J.; Darian, E.; Guvench, O.; Lopes, P.; Vorobyov, I.; MacKerell, A. D. Charmm General Force Field: A Force Field for Drug-Like Molecules Compatible with the Charmm All-Atom Additive Biological Force Fields. *J. Comput. Chem.* **2010**, *31*, 671−690.
(44) Ewald, P. P. Die Berechnung Optischer Und Elektrostatischer Gitterpotentiale. *Ann. Phys. (Berlin, Ger.)* **1921**, *369*, 253−287.
(45) Humphrey, W.; Dalke, A.; Schulten, K. Vmd: Visual Molecular Dynamics. *J. Mol. Graphics* **1996**, *14*, 33−38.

DOI: 10.1021/acsnano.6b02708
ACS Nano 2016, 10, 6905−6914